nature materials

LETTERS

PUBLISHED ONLINE: 9 MARCH 2015 | DOI: 10.1038/NMAT4232

Origami structures with a critical transition to bistability arising from hidden degrees of freedom

Jesse L. Silverberg[1*†], Jun-Hee Na[2†], Arthur A. Evans[3], Bin Liu[1], Thomas C. Hull[4], Christian D. Santangelo[3], Robert J. Lang[5], Ryan C. Hayward[2] and Itai Cohen[1]

Origami is used beyond purely aesthetic pursuits to design responsive and customizable mechanical metamaterials[1–8]. However, a generalized physical understanding of origami remains elusive, owing to the challenge of determining whether local kinematic constraints are globally compatible and to an incomplete understanding of how the folded sheet's material properties contribute to the overall mechanical response[9–14]. Here, we show that the traditional square twist, whose crease pattern has zero degrees of freedom (DOF) and therefore should not be foldable, can nevertheless be folded by accessing bending deformations that are not explicit in the crease pattern. These hidden bending DOF are separated from the crease DOF by an energy gap that gives rise to a geometrically driven critical bifurcation between mono- and bistability. Noting its potential utility for fabricating mechanical switches, we use a temperature-responsive polymer-gel version of the square twist to demonstrate hysteretic folding dynamics at the sub-millimetre scale.

A key theme unifying the study of biopolymer gels[15,16], biological tissues[17], kinematic mechanisms[18–21], granular media[22–24], network glasses[25] and architectural elements[26] is the competition between the number of internal DOF, N_f, and the number of internal mechanical constraints, N_c. The macroscopic behaviour of these systems in the absence of self-stresses[27,28] is said to be underconstrained when $N_f > N_c$, overconstrained when $N_f < N_c$, and isostatic, or marginally stable, when $N_f = N_c$. This framework, which was initially laid out by J. C. Maxwell in 1864, has been instrumental in understanding a diverse range of mechanical phenomena in constraint-based materials, including rigidity percolation[16], topologically protected zero energy modes[19], nonlinear elasticity[16] and shock waves[24]. A feature intrinsic to real physical materials but often left out of simpler models is the existence of a hierarchy of DOF, each with its own associated energy scale. When the details of these internal features are incorporated, systems can be overconstrained and rigid with respect to low-energy loading, but underconstrained and compliant as higher-energy DOF are accessed. Thus, N_f should be thought of as a variable quantity that changes with the experimental energy scale.

Although these observations are fairly general, the emergent mechanical phenomena that can be found in materials as the DOF hierarchy is probed has not been well examined. Indeed, this problem plays out in origami mechanics, where crease patterns that are mathematically unfoldable because $N_f \leq N_c$ nevertheless easily fold when made by hand[10,11,29,30]. In essence, the discrepancy originates when origami structures are modelled as a series of rigid polyhedra connected by freely rotating torsional hinges. Although rigid foldability appears to be a reasonable simplification for the folding behaviour, the fact that real materials can bend is a critical piece of missing phenomenology. In fact, there is at present no general approach for understanding and predicting the mechanical behaviour of origami structures when their material properties are taken into account. Although numerous examples of unfoldable crease patterns exist, we here investigate the mechanics of a single unit from the square-twist origami tessellation[1] (Fig. 1a,b; see also Supplementary Movies 1 and 2 and Supplementary Fig. 1). Even in this simple test case, we find a rich set of mechanical behaviours that illuminate general principles applicable to any material with measurably different energy scales separating overconstrained and underconstrained states.

The square-twist pattern consists of alternating square and rhombus facets, characterized by the length L and plane angle ϕ, in which the internal edges are either all mountain or valley creases. An analysis of the geometric constraints reveals the pattern is isostatic. Essentially, this arises from the four-fold rotational symmetry of the structure, which imposes a cyclic set of constraints on the four creases that define the central square facet (Supplementary Information). Although this observation indicates that the crease pattern should not be foldable, a trigonometric analysis of the normalized edge-to-edge distance x/L shows that the square twist allows two isolated states corresponding to the fully unfolded and folded configurations (Fig. 1c, upper and lower black lines, respectively, and Supplementary Fig. 2).

Experiments measuring x/L on folded paper sheets without external loading (Methods; Fig. 1c, red data points) indicate qualitatively different behaviour than the crease geometry's naive prediction of rigidity. Instead, below a critical plane angle $\phi_c = (25 \pm 2.5)^\circ$, the distinction between folded and unfolded configurations is not observed; the structure is monostable with an intermediate value of x/L (for example, Fig. 1b, side views). Above ϕ_c, both folded and unfolded configurations are observed; the folded configuration exhibits x/L values that nearly match the prediction, whereas the unfolded configuration exhibits x/L values that are smaller than predicted for ideal sheets (Fig. 1b, side view, and Fig. 1c). Although the crease pattern does not admit solutions between folded and unfolded branches for any $\phi > 0^\circ$, direct observations during the folding process reveal that the facets bend by a finite amount rather than remaining flat. These deformations are additional DOF hidden from the bare crease pattern, and are essential for foldability as they enable the structure to access otherwise geometrically forbidden configurations. It is the combination of this facet bending and the non-zero rest angles of the creases, which are plastically set when the sheet is fully folded, that gives rise to the observed intermediate configurations.

[1]Physics Department, Cornell University, Ithaca, New York 14853, USA. [2]Department of Polymer Science and Engineering, University of Massachusetts, Amherst, Massachusetts 01003, USA. [3]Department of Physics, University of Massachusetts, Amherst, Massachusetts 01003, USA. [4]Department of Mathematics, Western New England University, Springfield, Massachusetts 01119, USA. [5]Lang Origami, Alamo, California 94507, USA. †These authors contributed equally to this work. *e-mail: JLS533@cornell.edu

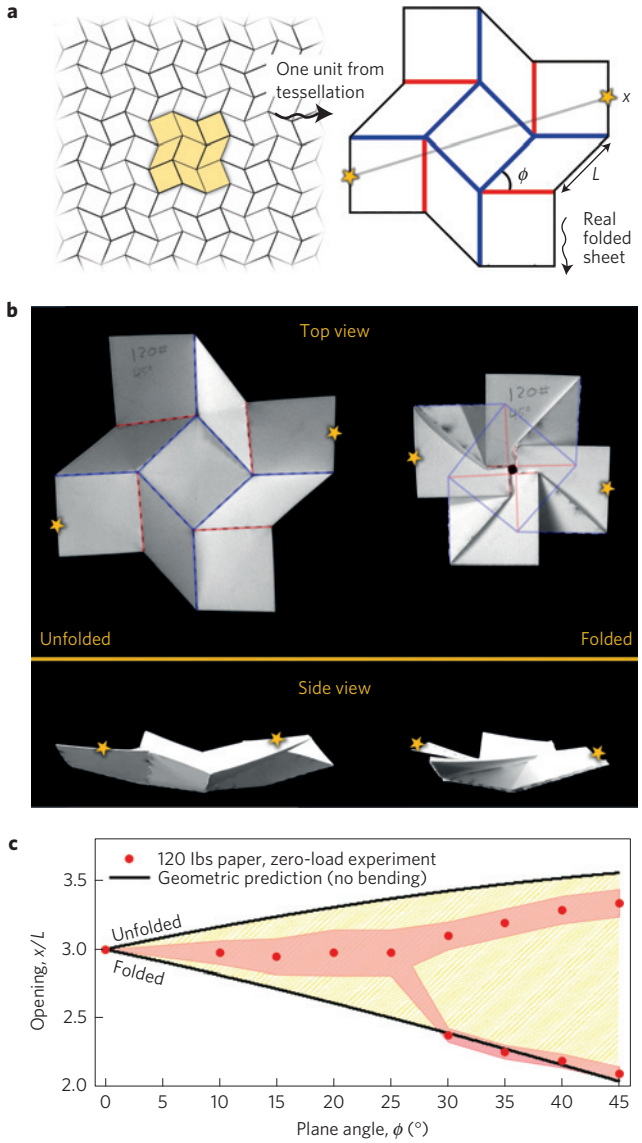

Figure 1 | Schematics and photographs introducing the square twist's essential geometric properties and mechanical characteristics. a, The square-twist folding pattern is shown with the edges in black, mountain creases in red, and valley creases in blue. The geometry is defined by the length, L, and the plane angle, ϕ. The Euclidean distance, x, between the two yellow stars quantifies the macroscopic configuration between folded and unfolded states. **b**, Photographs of a square twist with $\phi = 45°$ illustrate out-of-plane deformations, and the stars define x when the square twist is unfolded and folded. **c**, Comparison of geometric predictions to experimental measurements for x/L as a function of ϕ based purely on the crease pattern reveals qualitative disagreement. The former has bistable solutions for all non-zero ϕ corresponding to folded and unfolded configurations (black lines), and no permissible configurations between these two states (lightly shaded region between lines). Experimental measurements, however, exhibit regions with mono- and bistable solutions depending on ϕ (red points, errors are shaded bands).

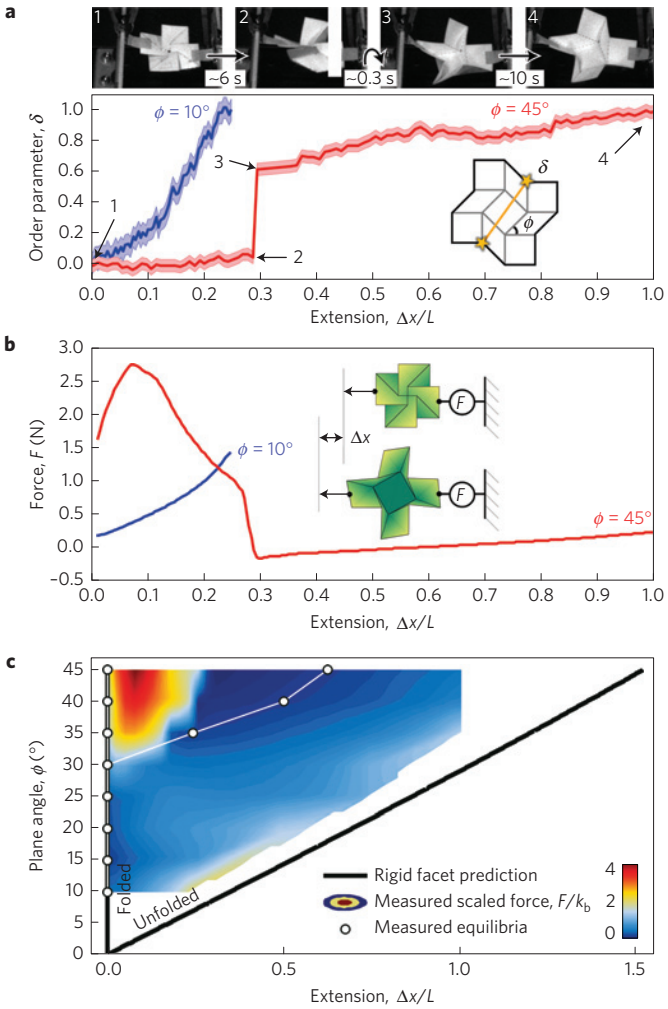

Figure 2 | Experimental strain-controlled mechanical data studying the transition between mono- and bistability in square twists. **a**, Measurements of the folding order parameter, δ, show smooth continuous behaviour for $\phi = 10°$ and an abrupt discontinuous jump for $\phi = 45°$. The inset illustrates the definition of δ, and photographs show points of interest on the red curve. **b**, Measurements of the tensile force F as a function of the normalized extension, $\Delta x/L$, reveal mechanical bistability between folded and unfolded configurations for $\phi = 45°$ and monostability for $\phi = 10°$. The inset shows schematics of the experiment, definition of Δx, and location of the load cell. **c**, Measurements of the tensile force, $F(\phi, \Delta x/L)$, normalized by the sheet's torsional bending stiffness, k_b, show the transition between mono- and bistability. White circles indicate mechanically stable values of $\Delta x/L$, and black lines show predicted solutions based on a crease geometry with rigid facets. Note that these predictions do not permit solutions anywhere off the lines. Furthermore, these data closely correspond to the measurements in Fig. 1c, where load-free stable values of x were plotted as red dots, and where the predicted solutions based on a rigid-facet geometry were similarly shown as black lines.

To study the unfolding behaviour, we measured the mechanical response of the folded square twist to uniaxial tension. We observe remarkably different behaviours for ϕ above and below the critical plane angle ϕ_c. Below ϕ_c, the structure smoothly opens and closes, as indicated by the folding order parameter δ (Fig. 2a inset and blue line; Supplementary Movie 1), whereas above ϕ_c a rapid snapping action between folded and unfolded states is observed, as indicated by a jump in δ (Fig. 2a, red line; Supplementary Movie 2). In the latter case, where $\phi > \phi_c$, both folded and unfolded configurations are stable to small external loading, whereas intermediate configurations are unstable and quickly snap to one state or the other. Displacement-controlled measurements of the force F as a function of ϕ and normalized extension $\Delta x/L$ also showed qualitatively different behaviour above and below ϕ_c (Fig. 2b and inset). Here, the extension Δx is the change in x at a given force F along the direction of loading (Methods). For structures with $\phi < \phi_c$ the force curves

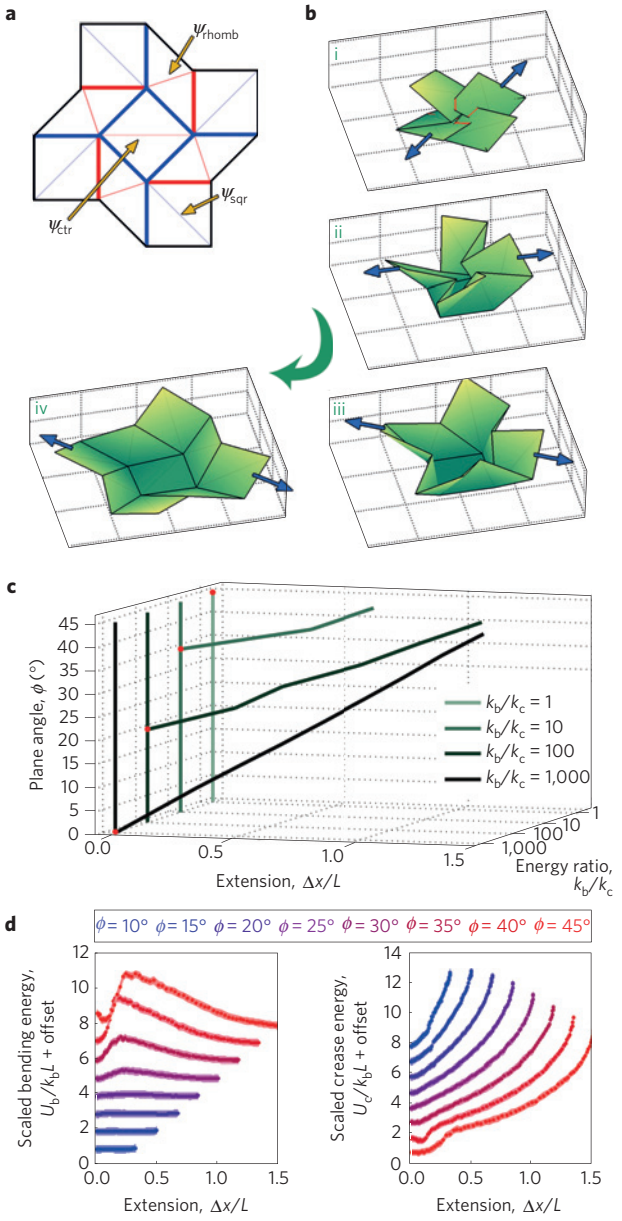

Figure 3 | Simulation results for the square twist with non-rigid facets. **a**, The square-twist crease diagram has been modified with 'virtual creases' that mimic the behaviour of facet bending, as indicated by thin lines. **b**, 3D renderings from the simulation illustrate the unfolding sequence. Blue arrows indicate the external load corresponding to strain-controlled conditions. **c**, Simulation data where each line represents the mechanically stable extensions as a function of geometry for various material properties. The data reveal a critical angle ϕ_c (red dots) that varies with the bending-to-crease energy ratio k_b/k_c. For $k_b/k_c = 1$, monostability is observed for all ϕ, whereas for $k_b/k_c = 10^3$ bistability is found for all ϕ. Between these limits, a bifurcation separating the monostable ($\phi < \phi_c$) and bistable ($\phi > \phi_c$) limits of the phase transition can be found. **d**, Examining the distribution of energy between crease and bending degrees of freedom for $k_b/k_c = 10^2$ as a typical example, we see that the contribution from bending has an energy barrier for intermediate values of $\Delta x/L$ that increases in magnitude with ϕ. Conversely, the energetic contribution from crease opening essentially increases monotonically with $\Delta x/L$ for all ϕ. In both energy plots, the band thickness indicates the simulation uncertainty.

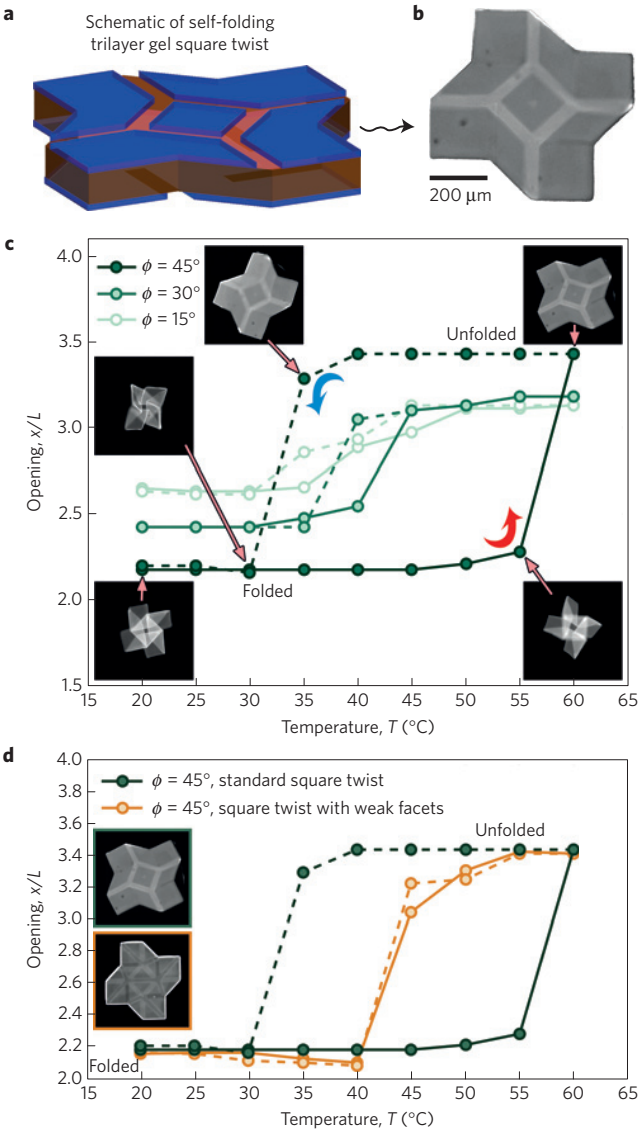

Figure 4 | A sub-millimetre-scale self-folding polymer-gel version of the square twist is used to verify the geometric nature of bistability in stress-controlled conditions. **a**, Schematic of the trilayer structure (dimensions not to scale). Folding is actuated by a temperature-dependent swelling of the middle (pink) layer. Open slits patterned in the top and bottom layers (blue) induce mountain and valley creases, respectively, when viewed from above. **b**, Optical micrograph of a square twist released in an aqueous medium at 60 °C. **c**, Measurements of square-twist opening as a function of temperature demonstrate hysteretic folding/unfolding behaviour for $\phi > \phi_c$ and non-hysteretic folding/unfolding for $\phi < \phi_c$. In this case, $15° < \phi_c < 30°$. Solid lines (unfolding) correspond to heating, and dashed lines (folding) to cooling. Inset micrographs show a structure with $\phi = 45°$ at the indicated measurement points. **d**, Measurements of opening as a function of temperature for the standard square twist compared to a version with creases added where bending would otherwise occur. The additional DOF afforded by setting $k_b/k_c \lesssim 1$ entirely remove hysteretic folding behaviour.

increase monotonically, whereas structures with $\phi > \phi_c$ exhibit force curves with regions of negative slope, indicating mechanical instability. To determine the force landscape that drives transitions from the folded to the unfolded state, we measured the tensile force normalized by the sheet's torsional bending stiffness, k_b (Fig. 2c, Supplementary Figs 3 and 4). We find that the force barrier between these states increases in magnitude with ϕ, hinting at an underlying mechanism for bistability. In particular, facet bending is localized to the rhombi short diagonals, forming 'virtual creases' with a deflec-

tion angle ψ and energy $\sim Lk_b \sin(\phi/2)\psi^2$. Because the length of these diagonals increases with ϕ, the force barrier increases as well.

To further investigate this facet-bending mechanism, we developed a numerical simulation of the unfolding behaviour under uniaxial tension that calculates the configuration minimizing the facet-bending and crease-unfolding energies for a given ϕ and $\Delta x/L$ (Fig. 3a,b, Methods). From these calculations, we determine the energetic minima, which correspond to mechanically stable states, for different ratios of the bending and crease torsional spring constants, k_b/k_c (Fig. 3c). For $k_b/k_c \leq 1$, monostability was observed for all geometries, whereas for $k_b/k_c \geq 10^3$, all geometries exhibited bistability. Between these limits, we found a critical plane angle ϕ_c marking a bifurcation between mono- and bistability that varied with k_b/k_c. When compared with the experimental phase diagram (Fig. 2c), these calculations predict $10 < k_b/k_c < 100$, which is consistent with measurements that found $k_b/k_c \simeq 36$ for the paper used in experiments (Supplementary Information).

Examining the internal distribution of energy by separating the dimensionless bending energy U_b/k_bL from the dimensionless crease energy U_c/k_bL sheds light on how different DOF are interacting to tune the bifurcation (Fig. 3d). For example, taking $k_b/k_c = 10^2$, where $\phi_c \approx 20°$, we see that the system's total bending energy has an energy barrier at intermediate values of $\Delta x/L$ whose magnitude increases with ϕ. The total crease energy, on the other hand, monotonically increases with $\Delta x/L$ for all ϕ. Whether this monotonic rise in crease energy is high enough to overcome the energy barrier that arises from hidden bending DOF determines if the system is mono- or bistable (Supplementary Fig. 5).

Collectively, these results provide a geometric understanding for the mechanical bistability of the square twist and, as such, should translate to any thin sheet folded according to this crease pattern. Although our experiments were performed with strain-controlled loading, we predict that the observed bifurcation will give rise to a hysteretic behaviour under stress-controlled loading that can be tuned by both ϕ and k_b/k_c. To test this prediction, we used a micropatterned gel-trilayer version of the square twist with $L = 200\,\mu m$ (Fig. 4a,b; Methods). Here, differential swelling between gel layers is used to create internal stresses that fold and unfold the structure as the temperature T is varied. For this system, we estimate $k_b/k_c \sim 10^2$ (Supplementary Information), and therefore from simulations we expect $\phi_c \approx 20°$ (Fig. 3c). Imaging a square twist with $\phi = 45°$ as the temperature is quasi-statically varied reveals the expected hysteresis (Fig. 4c, dark green line). As predicted, when ϕ is decreased to 30° the hysteresis is reduced (medium green line), and ultimately vanishes for $\phi = 15°$ (light green line). Our results with paper models and simulations also suggest that hysteretic folding behaviour can be removed if $k_b/k_c \lesssim 1$. This scenario can be realized in the gel sheets by modifying and fully triangulating the crease pattern (for example, Fig. 3a), effectively placing creases where bending would otherwise occur. Indeed, we find for $\phi = 45°$ that the addition of these creases removes the hysteresis (Fig. 4d). These experiments clearly illustrate the first-order properties of the transition between folded and unfolded states that arises from hidden bending DOF in the square twist (Supplementary Fig. 6).

Although this work shows how hidden DOF can be used to create non-trivial features in an origami structure's configuration space, we envisage that the tunable and scale-free nature of the square twist's bistability should make it a useful design for robotic grippers, microfluidic devices and even wearable exoskeletons. Moreover, because the square twist can form 2D tessellations, it should be possible to spatially vary the unit-cell geometry to create origami mechanical metamaterials. For example, in analogy with secondary structures in polymers that provide hidden length[31], the ability of the pattern to resist deformation up to a predetermined force threshold can be taken advantage of to make materials with extremely high toughness. Such devices would be capable of large bulk strain without fracture by absorbing energy in a predetermined pattern of sequentially opening square-twist unit cells. More broadly, the possibility of alternative geometries (Supplementary Fig. 7) and additional hidden DOF—such as facet stretching, facet shearing and crease torquing—suggests that an even richer configuration space may be hidden with these more energetically expensive deformation modes. For example, these ideas are found in the mechanics of thin shells, where bending and stretching energy barriers have been shown to be modified by the introduction of creases[32], leading to a broad range of multistable behaviours. Thus, the geometry of creased sheets offers a simple experimental platform to probe the mechanical behaviour of a wider class of constraint-based materials and the consequences of energy-scale dependent DOF.

Methods

Sample fabrication and characterization. Digital CAD software and a laser cutter were used to fabricate square-twist structures from 120 lb paper (Radiance 120 lb super smooth card stock, Beckett Expressions). Creases were patterned by cutting perforated lines with equal lengths of material and gaps, then folded by hand with a Lineco bone scorer to be mountain or valley according to the crease assignment (Fig. 1a). For these samples, we set $L = 2.54$ cm and varied ϕ from 10° to 45° in increments of 5°. The lower bound is the limit of what can be reasonably folded from this material, although a theoretical limit of 0° is where the crease pattern is no longer well defined owing to overlapping mountain and valley curves. The upper bound is set by self-intersection, which prevents the structure from folding flat for $\phi > 45°$. Samples used throughout this work were folded and unfolded before mechanical testing, thus the unfolded stable configuration retains some folding along the creases owing to plastic deformation and hence responds differently than a 'pristine' sheet that has never been folded.

To quantify a square twist's configuration in the absence of load, each sample was first folded flat, then held to a calliper ruler to measure the Euclidean distance x (Fig. 1a). Subsequently, each sample was unfolded, flattened on a table under 2 s of compression applied by hand, and the distance x remeasured.

A custom-built mechanical tester previously described[5] was used to measure the mechanical properties of square twists under tension. Samples were fixed to the testing device and suspended in air with small tabs of gaffing tape. Although this pre-loaded the samples with minor tension at zero extension (Fig. 2a), this approach prevented any interactions with the lower surface of the testing apparatus, which would otherwise interfere with the unfolding process. In a typical experiment, the distance between loading plates and load cell force data were simultaneously recorded by a single custom MATLAB program, and the data stored for later analysis. Furthermore, the maximum experimental extension was kept smaller than the theoretical limits (Fig. 2c black lines) to reduce risk of tearing samples apart. Sample testing was video recorded with a Canon Powershot camera filming at 7.5 FPS. Standard image analysis techniques were used to measure the order parameter for folding, δ, as a function of the normalized extension $\Delta x/L$, which as described in the main text is measured from the mechanically equilibrated folded state (Fig. 1c lower branch of red data).

Simulated square twists. To explore how material properties, and in particular finite bending stiffness of the flat facets, influences mechanical behaviour of the system, we developed a numerical simulation of the square twist's folding behaviour. In it, we constrained each of the 16 facet corners to have a fixed distance from their neighbouring corners according to the crease pattern. Crease and facet bending deformations were then assigned an elastic energy given by:

$$\begin{aligned} U_{\text{total}} &= U_{\text{crease}} + U_{\text{bend}} \\ &= \frac{L}{2}\left[k_c \sum_{i=1}^{12} (\theta_i - \theta_0)^2 + k_b \sum_{j=1}^{9} \lambda_j \psi_j^2\right] \end{aligned} \tag{1}$$

where

$$\lambda_j = \begin{cases} \sqrt{2} & \text{for square facets,} \\ 2\sin(\phi/2) & \text{for rhombus facets} \end{cases}$$

In this expression, the first term is the crease energy, which is proportional to the torsional elastic constant k_c times the crease length L, and is a sum over the 12 individual creases. It is also a function of the crease angle θ, determined from a dot product of two adjacent facet normals, minus an equilibrium value θ_0. This represents the fact that, once made, creases no longer lay flat. A value of $\theta_0 = 10°$ was used here, which is consistent with our experimental samples. The second term is the facet-bending energy, which is proportional to the torsional elastic constant k_b times the length of the bend $\lambda_j L$, and is a sum over the nine indicated facet diagonals (Fig. 3a). It is a function of the bending angle ψ_j, which, unlike creases, is zero in a stress free state. Like the crease DOF, these bending DOF are also calculated from the dot product of the facet normals.

Specifying ϕ and a target $\Delta x/L$, equation (1) was numerically minimized using the Levenberg–Marquardt algorithm in MATLAB, where the target $\Delta x/L$ was incremented from 0 to its maximum value in 91 steps. This process was repeated 20 times with initial conditions generated from a geometric interpolation between the folded and unfolded states that did not preserve facet areas. In each realization, the facet corners were perturbed along x, y and z by an amount that was uniformly distributed over the range given by $\pm L/10$. In this way, we used semi-random initial conditions to form an ensemble-averaged solution that minimized equation (1) and satisfied the crease pattern's geometric constraints. We then averaged the facet bending angles of the ensemble-averaged solution, producing an overall average rhombus bending angle ψ_{rhomb}, an overall average square-facet bending angle ψ_{sqr}, and a centre square-facet bending angle ψ_{ctr} (Supplementary Information).

Self-folding gel fabrication and imaging. The self-folding version of the square twist consists of a temperature-responsive hydrogel film capped on both the top and bottom surfaces by rigid patterned layers. Although the method is described elsewhere[33], we provide a brief summary here. First, we spin-coated a layer of ultraviolet-crosslinkable poly(*p*-methyl styrene) (PpMS) with a thickness of 50 nm. Using a maskless lithographic method, a pattern of stripes corresponding to the valley creases was used to define regions where the PpMS layer was crosslinked. Next, the temperature-responsive poly(*N*-isopropyl acrylamide-*co*-sodium acrylate) (PNIPAM) polymer was deposited and crosslinked on the PpMS layer with a thickness of 1.5 µm. Finally, a second layer of PpMS with a thickness of 50 nm was deposited and crosslinked with a pattern corresponding to the mountain creases. This trilayer structure then consisted of two thin rigid outer layers encompassing a middle layer that swells with temperature. To prevent adhesion between the hydrophobic PpMS panels in the folded state, a 10-nm polyelectrolyte layer was coated on both outer surfaces of PpMS by spin-coating a photo-crosslinkable poly(sulphopropyl methacrylate) copolymer and crosslinking with ultraviolet light. On swelling in an aqueous buffer, stresses are developed within the middle hydrogel layer, causing the bilayer crease-like regions to bend to an angle programmed by the width of the open stripe in the capping PpMS layer. Trilayer regions, on the other hand, remain flat like facets. For the square-twist pattern, each crease segments is programmed to fold to either $\pm\pi$ at room temperature, corresponding to the flat folded state.

Full triangulation of the fold pattern was accomplished by patterning open stripes in both the top and bottom rigid films where bending was observed in the paper experiments and numerical simulations. Thus, these regions had only a single layer gel film that was not programmed to fold, but instead offered much lower bending resistance than the trilayer facet regions.

To measure the opening x, each sample was placed in an aqueous medium and observed with epi-fluorescence microscopy through the temperature range 20 to 60 °C. A heat stage was used to control the temperature (Zeiss Tempcontrol 37-2 digital), which was varied in 5 °C increments. At least 30 min at each temperature was allowed for the gel to swell to equilibrium. The folding/unfolding process, therefore, was under quasi-static stress-controlled conditions. 3D images of polymer square twist were reconstructed using ImageJ from image stacks collected using a laser scanning confocal fluorescence microscope (Zeiss LSM 510 META), with the refractive index of the aqueous medium corrected for.

Received 28 November 2014; accepted 30 January 2015; published online 9 March 2015; corrected after print 31 March 2015

References

1. Greenberg, H., Gong, M., Magleby, S. & Howell, L. Identifying links between origami and compliant mechanisms. *Mech. Sci.* **2,** 217–225 (2011).
2. Song, J., Chen, Y. & Lu, G. Axial crushing of thin-walled structures with origami patterns. *Thin. Walled Struct.* **54,** 65–71 (2012).
3. Schenk, M. & Guest, S. D. Geometry of miura-folded metamaterials. *Proc. Natl Acad. Sci. USA* **110,** 3276–3281 (2013).
4. Wei, Z. Y., Guo, Z. V., Dudte, L., Liang, H. Y. & Mahadevan, L. Geometric mechanics of periodic pleated origami. *Phys. Rev. Lett.* **110,** 215501 (2013).
5. Silverberg, J. L. *et al.* Using origami design principles to fold reprogrammable mechanical metamaterials. *Science* **345,** 647–650 (2014).
6. Waitukaitis, S., Menaut, R., Chen, B. G-g. & van Hecke, M. Origami multistability: From single vertices to metasheets. *Phys. Rev. Lett.* **114,** 055503 (2015).
7. Lv, C., Krishnaraju, D., Konjevod, G., Yu, H. & Jiang, H. Origami based mechanical metamaterials. *Sci. Rep.* **4,** 5979–5981 (2014).
8. Hanna, B. H., Lund, J. M., Lang, R. J., Magleby, S. P. & Howell, L. L. Waterbomb base: A symmetric single-vertex bistable origami mechanism. *Smart Mater. Struct.* **23,** 094009 (2014).
9. Huffman, D. A. Curvature and creases: A primer on paper. *IEEE Trans. Comput.* **25,** 1010–1019 (1976).
10. Tachi, T. in *Proceedings of the International Association for Shell and Spatial Structures (IASS) Symposium: Evolution and Trends in Design, Analysis and Construction of Shell and Spatial Structures* (eds Domingo, A. & Lazaro, C.) 2287–2294 (Editorial Universitat Politècnica de València, 2009); http://go.nature.com/HbzSH1
11. Hull, T. *Project Origami: Activities for Exploring Mathematics* (CRC Press, 2012).
12. Thiria, B. & Adda-Bedia, M. Relaxation mechanisms in the unfolding of thin sheets. *Phys. Rev. Lett.* **107,** 025506 (2011).
13. Dias, M. A., Dudte, L. H., Mahadevan, L. & Santangelo, C. D. Geometric mechanics of curved crease origami. *Phys. Rev. Lett.* **109,** 114301 (2012).
14. Lechenault, F., Thiria, B. & Adda-Bedia, M. Mechanical response of a creased sheet. *Phys. Rev. Lett.* **112,** 244301 (2014).
15. Feng, S. & Sen, P. N. Percolation on elastic networks: New exponent and threshold. *Phys. Rev. Lett.* **52,** 216–219 (1984).
16. Broedersz, C. P., Mao, X., Lubensky, T. C. & MacKintosh, F. C. Criticality and isostaticity in fibre networks. *Nature Phys.* **7,** 983–988 (2011).
17. Silverberg, J. L. *et al.* Structure-function relations and rigidity percolation in the shear properties of articular cartilage. *Biophys. J.* **107,** 1–10 (2014).
18. Sun, K., Souslov, A., Mao, X. & Lubensky, T. Surface phonons, elastic response, and conformal invariance in twisted kagome lattices. *Proc. Natl Acad. Sci. USA* **109,** 12369–12374 (2012).
19. Kane, C. & Lubensky, T. Topological boundary modes in isostatic lattices. *Nature Phys.* **10,** 39–45 (2013).
20. Chen, B. G-g., Upadhyaya, N. & Vitelli, V. Nonlinear conduction via solitons in a topological mechanical insulator. *Proc. Natl Acad. Sci. USA* **111,** 13004–13009 (2014).
21. Paulose, J., Chen, B. G-g. & Vitelli, V. Topological modes bound to dislocations in mechanical metamaterials. *Nature Phys.* **11,** 153–156 (2015).
22. Liu, A. J. & Nagel, S. R. Nonlinear dynamics: Jamming is not just cool any more. *Nature* **396,** 21–22 (1998).
23. Keys, A. S., Abate, A. R., Glotzer, S. C. & Durian, D. J. Measurement of growing dynamical length scales and prediction of the jamming transition in a granular material. *Nature Phys.* **3,** 260–264 (2007).
24. Van den Wildenberg, S., van Loo, R. & van Hecke, M. Shock waves in weakly compressed granular media. *Phys. Rev. Lett.* **111,** 218003 (2013).
25. Thorpe, M. Continuous deformations in random networks. *J. Non-Cryst. Solids* **57,** 355–370 (1983).
26. Heyman, J. *The Science of Structural Engineering* (World Scientific, 1999).
27. Maxwell, J. C. On the calculation of the equilibrium and stiffness of frames. *Lond. Edinb. Dubl. Phil. Mag. J. Sci.* **27,** 294–299 (1864).
28. Calladine, C. Buckminster Fuller's "tensegrity" structures and Clerk Maxwell's rules for the construction of stiff frames. *Int. J. Solids Struct.* **14,** 161–172 (1978).
29. Demaine, E. D., Demaine, M. L., Hart, V., Price, G. N. & Tachi, T. (Non) existence of pleated folds: How paper folds between creases. *Graphs Combinator.* **27,** 377–397 (2011).
30. Hull, T. C. *Origami*^{3}*: Proceedings of the Third International Meeting of Origami Science, Mathematics, and Education* 29–38 (A K Peters, 2002).
31. Fantner, G. E. *et al.* Sacrificial bonds and hidden length: Unraveling molecular mesostructures in tough materials. *Biophys. J.* **90,** 1411–1418 (2006).
32. Bende, N. P. *et al.* Geometrically controlled snapping transitions in shells with curved creases. Preprint at http://arxiv.org/abs/1410.7038 (2014).
33. Na, J-H. *et al.* Programming reversibly self-folding origami with micropatterned photo-crosslinkable polymer trilayers. *Adv. Mater.* **27,** 79–85 (2015).

Acknowledgements

The authors thank J. Mosely, U. Nguyen, B. Johnson, B. Parker and M. Schneider for artistic inspiration, as well as O. Vincent, N. Bende, C-K. Tung, S. Waitukaitis and the Cohen lab for useful discussions. We also thank F. Parish for assistance with the laser cutter. This work was funded by the National Science Foundation through award EFRI ODISSEI-1240441.

Author contributions

J.L.S., J-H.N., R.C.H. and I.C. designed the research; J.L.S., J-H.N. and A.A.E. conducted the research and interpreted the results; B.L., T.C.H., C.D.S., R.J.L., R.C.H. and I.C. supervised the research and interpreted the results; J.L.S., J-H.N., A.A.E., T.C.H., R.J.L. and I.C. prepared the manuscript.

Additional information

Supplementary information is available in the online version of the paper. Reprints and permissions information is available online at www.nature.com/reprints. Correspondence and requests for materials should be addressed to J.L.S.

Competing financial interests

The authors declare no competing financial interests.

CORRIGENDUM

Origami structures with a critical transition to bistability arising from hidden degrees of freedom

Jesse L. Silverberg, Jun-Hee Na, Arthur A. Evans, Bin Liu, Thomas C. Hull, Christian D. Santangelo, Robert J. Lang, Ryan C. Hayward and Itai Cohen

Nature Materials **14,** 389–393 (2015); published online 9 March 2015; corrected after print 31 March 2015.

In the version of this Letter originally published, the authors Jesse L. Silverberg and Jun-Hee Na should have been denoted as having contributed equally to this work. This has now been corrected in the online versions of the Letter.